ACS Catalysis

Research Article

Cite This: ACS Catal. 2019, 9, 2854−2865

pubs.acs.org/acscatalysis

Enzymatic Carboxylation of 2-Furoic Acid Yields 2,5-Furandicarboxylic Acid (FDCA)

Karl A.P. Payne,[†] Stephen A. Marshall,[†] Karl Fisher,[†] Matthew J. Cliff,[†] Diego M. Cannas,[‡] Cunyu Yan,[†] Derren J. Heyes,[†] David A. Parker,[§] Igor Larrosa,[‡] and David Leys*[,†]

[†]Manchester Institute of Biotechnology, University of Manchester, 131 Princess Street, Manchester M1 7DN, U.K.

[‡]School of Chemistry, University of Manchester, Chemistry Building, Oxford Road, Manchester M13 9PL, U.K.

[§]Innovation/Biodomain, Shell International Exploration and Production, Westhollow Technology Center, 3333 Highway 6 South, Houston, Texas 77082-3101, United States

Supporting Information

ABSTRACT: The biological production of FDCA is of considerable value as a potential replacement for petrochemical-derived monomers such as terephthalate, used in polyethylene terephthalate (PET) plastics. HmfF belongs to an uncharacterized branch of the prenylated flavin (prFMN) dependent UbiD family of reversible (de)carboxylases and is proposed to convert 2,5-furandicarboxylic acid (FDCA) to furoic acid in vivo. We present a detailed characterization of HmfF and demonstrate that HmfF can catalyze furoic acid carboxylation at elevated CO_2 levels in vitro. We report the crystal structure of a thermophilic HmfF from *Pelotomaculum thermopropionicum*, revealing that the active site located above the prFMN cofactor contains a furoic acid/FDCA binding site composed of residues H296-R304-R331 specific to the HmfF branch of UbiD enzymes. Variants of the latter are compromised in activity, while H296N alters the substrate preference to pyrrole compounds. Solution studies and crystal structure determination of an engineered dimeric form of the enzyme revealed an unexpected key role for a UbiD family wide conserved Leu residue in activity. The structural insights into substrate and cofactor binding provide a template for further exploitation of HmfF in the production of FDCA plastic precursors and improve our understanding of catalysis by members of the UbiD enzyme family.

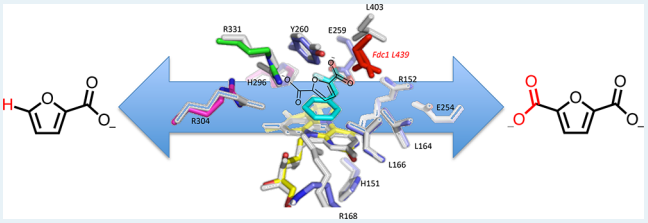

KEYWORDS: *2,5-furandicarboxylic acid, decarboxylase, enzyme mechanism, enzyme structure, flavin chemistry, prFMN, carboxylation*

Furan-based components such as 2,5-furandicarboxylic acid are of considerable value as potential (bio)replacements for petrochemical-derived monomers such as terephthalate, which are used in polymers such as polyethylene terephthalate (PET) plastics.[1,2] A chemical synthesis process for the carboxylation of furoic acid to FDCA has been recently reported, using molten cesium salts at 200−350 °C.[3] Furfural, the precursor to furoic acid, can be readily produced by acid-catalyzed thermohydrolysis of hemicellulosic material, a process that is already carried out on an industrial scale.[4,5]

A number of organisms are known to not only degrade furfural and hydroxymethylfurfural (HMF) but also utilize these as their sole carbon source.[6] The pathway and associated genes for furfural and HMF degradation were first identified in the Gram-negative bacterium *Cupriavidus basilensis* HMF14.[7] The genes are organized in two distinct clusters: HmfA−E, which are essential for both furfural and HMF degradation, and HmfF−H, which are required for HMF degradation only. The key step linking the HMF and furfural degradation pathways involved the decarboxylation of 2,5-furandicarboxylic acid (FDCA) to furoic acid (Figure 1a).[7] This decarboxylation step has been shown to be dependent on two gene products, HmfF and HmfG, which are homologous to *E. coli* UbiD and UbiX, respectively. The UbiD family of enzymes catalyze the reversible nonoxidative decarboxylation of a wide range of aromatic and unsaturated aliphatic compounds and are dependent for this activity on prenylated-FMN (prFMN).[8,9] The latter is synthesized by the prenyltransferase UbiX from reduced FMN and dimethylallylphosphate (DMAP).[10] The cofactor prFMN has been suggested to catalyze (de)-carboxylation via formation of a transient 1,3-dipolar cycloaddition adduct with the unsaturated substrate.[11] While certain UbiD family members (Figure 1b and Figure S1) function to carboxylate aromatic hydrocarbons in vivo, most UbiD-like enzymes act as decarboxylases in vivo.[12] However, many of those that function physiologically as decarboxylases have been shown to catalyze carboxylation in vitro when in the presence of excess bicarbonate as a source of CO_2.[11,13,14]

Received: December 5, 2018
Revised: February 6, 2019
Published: February 15, 2019

DOI: 10.1021/acscatal.8b04862
ACS Catal. 2019, 9, 2854−2865

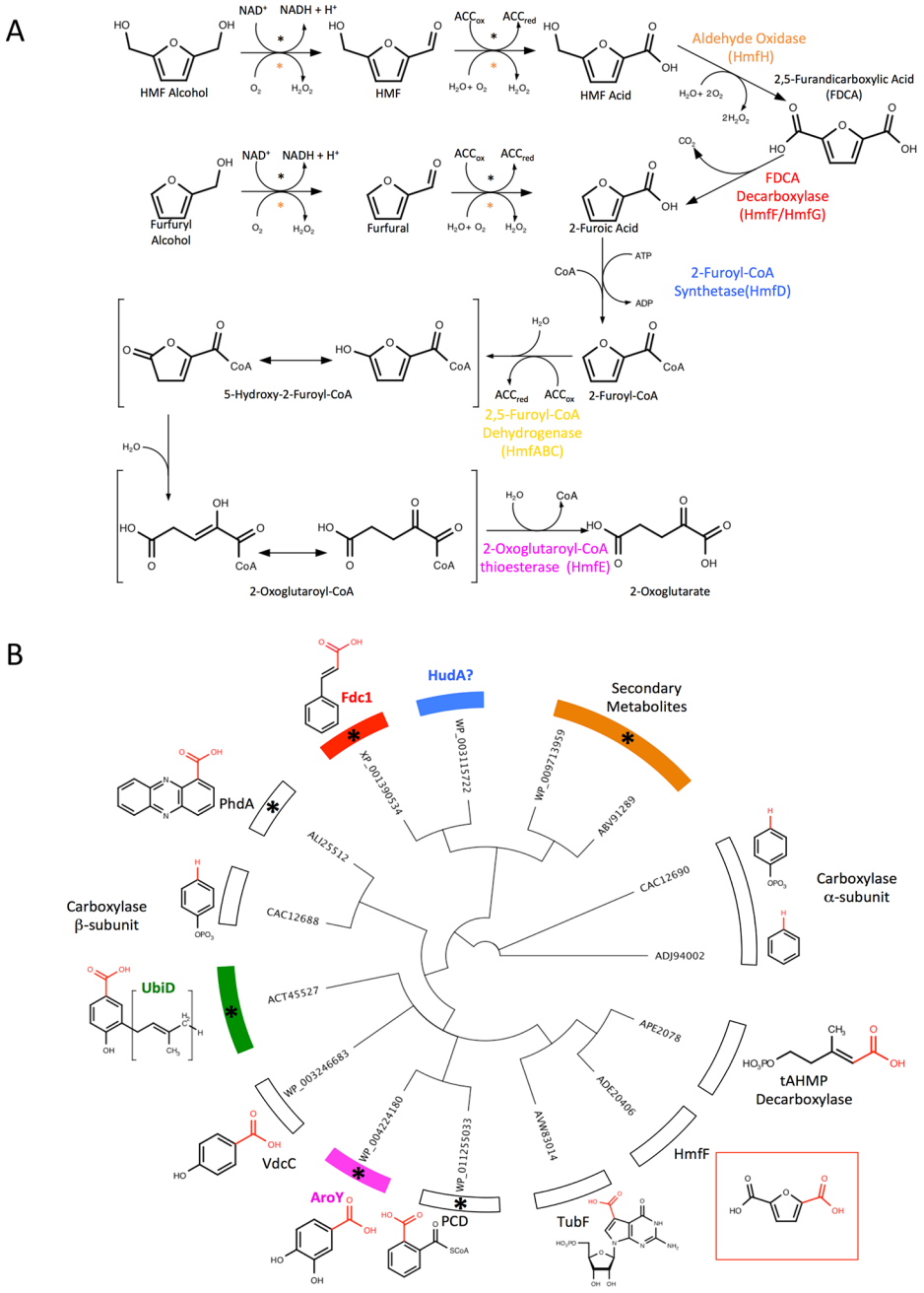

Figure 1. (A) Schematic for the *C. basilensis* furfural and 5-hydroxymethylfurfural (HMF) degradation pathway.[7] Oxidation steps in the upper part of the furfural and HMF pathway may be catalyzed either by HmfH (orange asterisks) or by other nonspecific dehydrogenases (black asterisks). ACC = electron acceptor, either oxidized (ACC_{ox}) or reduced (ACC_{red}). (B) Overview of the UbiD enzyme family: a phylogenetic tree of the characterized UbiD homologues. The different branches can be grouped by substrate specificity indicated by a representative substrate for the distinct groups. Groups for which crystal structures are available are highlighted in color, while an asterisk indicates prFMN confirmed as cofactor. HmfF belongs to a distinct branch that is located close to the recently discovered tAHMP decarboxylase.

Hence, we sought to understand whether HmfF can catalyze reversible decarboxylation and demonstrate if it could produce FDCA via carboxylation of furoic acid. Enzymatic FDCA production has been reported starting from HMF and utilizing oxidoreductases such as HmfH.[15] HmfF belongs to an uncharacterized branch of the UbiD family and is most similar to the recently discovered *trans*-anhydromevalonate 5-phosphate decarboxylase (tAHMPDC) involved in a novel archaeal mevalonate pathway (Figure 1b).[16]

In this paper we detail the biochemical characterization and structure determination of HmfF from the thermophilic organism *Pelotomaculum thermopropionicum*. The insights into prFMN-dependent carboxylation of furoic acid under high $[CO_2]$ conditions will support further exploitation of this enzyme in the production of FDCA.

RESULTS AND DISCUSSION

Initial Identification, Expression, and Characterization of Thermostable FDCA (De)carboxylases. It has previously been reported that the thermophilic bacterium *Geobacillus kaustophilus* HTA426 is capable of degrading furfural.[17] A BLAST search of the *G. kaustophilus* genome[18]

DOI: 10.1021/acscatal.8b04862
ACS Catal. 2019, 9, 2854−2865

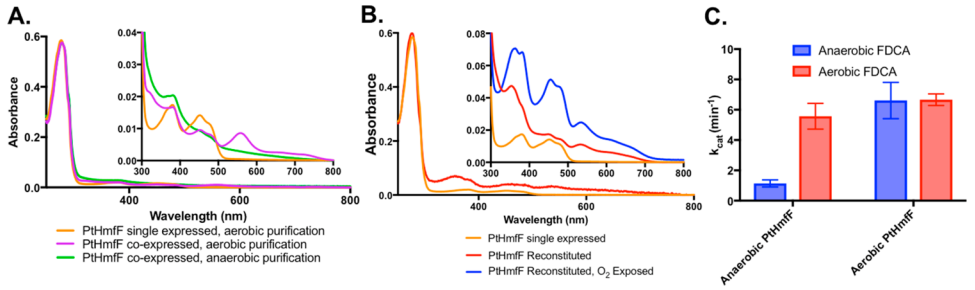

Figure 2. HmfF spectral properties, in vitro reconstitution, and oxygen dependence of activity. (A) UV−vis spectra obtained for heterologous expressed *P. thermopropionicum* HmfF. Spectra are shown of the WT protein expressed on its own (orange line) or coexpressed with UbiX and purified either aerobically (purple) or anaerobically (green). Spectra were normalized on the A_{280} peak. The inset shows the closeup of the cofactor-related spectral features present in the 300−800 nm region. (B) UV−vis spectra of single expressed "apo" *P. thermopropionicum* HmfF as isolated (orange), following reconstitution with in vitro synthesized prFMN under anaerobic conditions (red), and following exposure to air (blue). (C) Activity of reconstituted PtHmfF against aerobic or anaerobic substrate before and after exposure to air. Assays were performed against 900 μM FDCA at 25 °C (error bars represent SEM, n = 3).

using the *C. basilensis* Hmf gene cluster suggested the presence of a similar Hmf gene cluster located on plasmid pHTA426. Although there is no mention in the literature regarding the ability of *G. kaustophilus* to degrade HMF, a *C. basilensis* HmfF homologue (WP_011229502) could be located on pHTA426, possessing 51% sequence identity and located adjacent to a HmfG/UbiX homologue. Active recombinant *G. kaustophilus* HmfF was successfully produced in *E. coli* when it was coexpressed with *E. coli* UbiX (Figure S2). However, while soluble recombinant *G. kaustophilus* HmfF could be produced, the protein had a tendency to aggregate, hampering crystallogenesis and other biophysical studies. Other thermophilic HmfF homologues were screened, with the *P. thermopropionicum* HmfF enzyme being the most promising in terms of protein expression levels and stability. The purified recombinant HmfF enzymes (from both *P. thermopropionicum* and *G. kaustophilus*) were capable of decarboxylating 2,5-furandicarboxylic acid to furoic acid in vitro (Figure S2b) but could not further decarboxylate furoic acid to furan.

Expression and Detailed Characterization of *P. thermopropionicum* HmfF. Purified PtHmfF expressed in absence of *E. coli* UbiX coexpresssion was pale yellow and possessed a UV−vis spectrum consistent with oxidized FMN binding. In contrast, when it was coexpressed with UbiX, the purified recombinant protein was pale pink, possessing a complex UV−vis spectrum with three main features in addition to the protein peak at 280 nm (Figure 2A). These include a feature at 390 nm, similar to that observed previously for the model system *A. niger* Fdc1,[11] a peak at 450 nm (likely corresponding to the presence of a subpopulation bound to oxidized FMN rather than prFMN), and a broad peak centered around 550 nm. Similar spectral features at 550 nm were previously identified as corresponding to the semiquinone radical form of the prFMN cofactor.[11,13,19]

***P. thermopropionicum* HmfF in Vitro Reconstitution Confirms Oxidative Maturation Is Required for Activity.** While UbiX produces prFMN in a reduced state, the cofactor must undergo oxidative maturation within UbiD to produce the active prFMN^{iminium} form.[8−11] To investigate the requirement for oxidative maturation of the cofactor in HmfF, *apo*-enzyme was reconstituted in vitro as described previously for AroY and UbiD.[13,19] Single expressed HmfF lacking decarboxylation activity was reconstituted under anaerobic conditions and revealed prominent features at 360 and 530 nm (Figure 2B). Exposure to air resulted in an enhancement of the spectral features at 360−380, 450, and 530 nm, a range of spectral features suggestive of a mixture of normal oxidized FMN, prFMN^{radical}, and possibly prFMN^{iminium}, similar to that observed in the as isolated coexpressed enzyme. Consistent with this, the anaerobic reconstituted protein displayed low levels of decarboxylase activity when it was assayed under anaerobic conditions. However, the rate of enzymatic decarboxylation was 5-fold higher when the protein was assayed under aerobic conditions (Figure 2C). Taken together, these data confirm that, as with Fdc1 and AroY, HmfF requires oxidative maturation of prFMN for activity.

***Pt*HmfF Is Light and Oxygen Sensitive.** The activity of the as-isolated coexpressed *Pt*HmfF was found to rapidly decrease over time when it was stored on ice. The loss in activity appeared to be partially due to light exposure, with the half-life of *Pt*HmfF increasing from 35 to ∼100 min when it was stored in the dark under aerobic conditions (Figure S3). Similar observations were made for the *A. niger* Fdc1 enzyme, where light exposure was found to induce a complex isomerization of the cofactor leading to inactivation.[20] However, unlike Fdc1, protection from illumination was not sufficient to stabilize *Pt*HmfF activity. In contrast, *Pt*HmfF stored under anaerobic conditions did not appear to lose activity over the course of several hours, suggesting that inactivation was also the result of O_2, as observed for AroY.[13] Subsequently, *Pt*HmfF was either purified anaerobically or purified aerobically and then reconstituted in vitro and assayed under anaerobic conditions. The *Pt*HmfF enzyme activity was found to have a pH optimum between 6 and 6.5, with a temperature maximum of ∼60 °C (Figure 3). However, from 55 °C and above the activity decreased rapidly over the course of a few minutes, indicating that the enzyme was being inactivated, making it difficult to obtain accurate initial rates. Thermal denaturation of *Pt*HmfF monitored using CD spectroscopy revealed a melting temperature of ∼68 °C (Figure S4). Thus, all subsequent assays were performed at 50 °C. An Arrhenius plot of the 25−50 °C data points indicated an activation energy of 80.7 kJ mol^{-1}. At pH 6 and 50 °C, the apparent K_m and k_{cat} values for FDCA were 49.4(±3.7) μM and 2.39(±0.05) s^{-1}, respectively (Figure 3C). The *Pt*HmfF enzyme was also found to have minor activity with 2,5-pyrroledicarboxylic acid (PDCA). In contrast, no decarboxylation could be detected for 2,3-furandicarboxylic acid, 5-formyl-2-furoic acid, 5-hydroxymethyl-2-furoic acid, 5-nitro-2-furoic acid, 2,5-thiophenedicarboxylic acid, 2,6-pyridinedicar-

DOI: 10.1021/acscatal.8b04862
ACS Catal. 2019, 9, 2854−2865

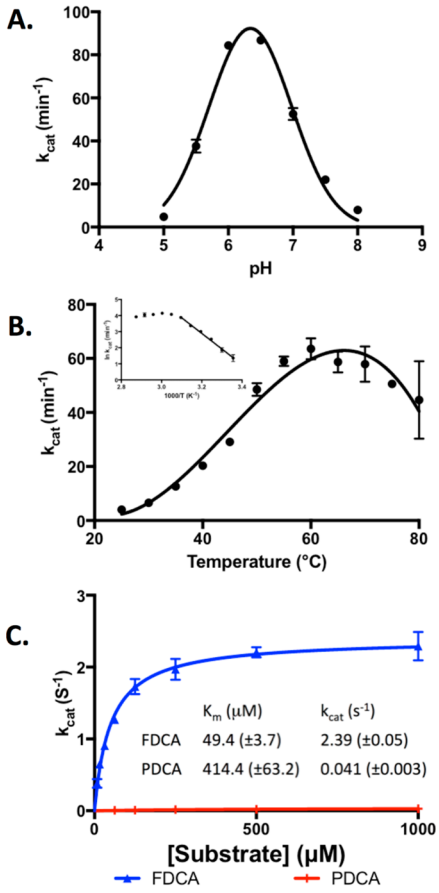

Figure 3. *Pt*HmfF enzyme activity. (A) Effect of pH on activity. (B) Effect of temperature on activity. Inset: Arrhenius plot of data. (C) Steady-state kinetic parameters obtained for *P. thermopropionicum* HmfF against FDCA (blue) and PDCA (red) at 50 °C and pH 6. Error bars represent SEM, n = 3.

boxylic acid, terephthalic acid, isophthalic acid, or muconic acid.

***Pt*HmfF Catalyzes H/D Exchange of a Small Range of Heteroaromatic Acids.** It has previously been shown that UbiD enzymes are capable of catalyzing deuterium exchange of substrates that can undergo UbiD-mediated carboxylation.[20,21] ^{1}H NMR showed that incubation of furoic acid with *Pt*HmfF in D_2O resulted in depletion of the resonance peak at 7.6 ppm consistent with exchange of the proton in the 5-position (denoted H_a) with a deuteron (Figure S5). This was further supported by a change in splitting of the 6.5 ppm resonance (corresponding to H_b) from a doublet of doublets to a doublet resulting from the loss of coupling between H_b and H_a. Partial H/D exchange of the 5-position of pyrrole-2-carboxylate (~30%, Figure S4B) could also be observed under the conditions tested; however, no exchange of thiophene-2-carboxylate was detected (Figure S5C). These observations confirm that the level of H/D exchange follows the same trend as observed for the level of decarboxylation of the corresponding diacids. With this in mind, we used H/D exchange to assay *Pt*HmfF against substrates where the corresponding diacids were not commercially available. The proton in the 5-position of 2-oxazolecarboxylic acid could only be readily exchanged for deuterium in the presence of enzyme (Figure S5D). In contrast, no enzyme-dependent exchange could be observed for position 2 of 5-oxazolecarboxylic acid (Figure S5E).

***Pt*HmfF and *Gk*HmfF Catalyze Furoic Acid Carboxylation at Elevated [CO_2].** The HmfF reverse reaction, carboxylation, has been demonstrated to occur in vivo for distinct UbiD members that function as dedicated carboxylases,[22−24] while those family members that act as decarboxylases under physiological conditions (such as AroY and Fdc1) can catalyze carboxylation in vitro at elevated levels of CO_2.[11,13,14] To investigate the ability of HmfF enzymes to catalyze the reverse reaction, carboxylation of furoic acid to produce FDCA, purified *Pt*HmfF and *Gk*HmfF enzymes were incubated with 50 mM furoic acid and 1 M bicarbonate at 50 °C overnight. HPLC analysis of the reaction mixtures revealed a peak with retention time of 2.3 min that comigrates with an FDCA standard (Figure 4A). Mass spectrometry confirmed that this species had a mass of 154.99 Da, consistent with the expected mass for FDCA. We sought to determine whether performing the reaction under pressurized CO_2 could increase the amount of carboxylated product. Reaction mixtures containing 50 mM furoic acid were incubated overnight with HmfF at 50 °C. In the presence of 1 M $KHCO_3$, there was no significant difference between reaction mixtures incubated under N_2 at atmospheric pressure or under CO_2 at 32 bar with ~2 mM FDCA produced. In the absence of bicarbonate, ~150 μM FDCA was produced under 32 bar CO_2, whereas no FDCA was detectable under N_2 (Figure 4B). While HmfF presents an attractive route to the production of 2,5-furandicarboxylic acid, a potential bioreplacement for polymer precursors, yields remain low even under high [CO_2]. Given the unfavorable equilibrium for the carboxylation reaction, future efforts aimed at increasing the yield for this reaction will likely require in situ conversion of FDCA.

***Pt*HmfF Crystal Structures Reveal FMN Binding Mode.** To aid crystallization, the *Pt*HmfF was expressed without affinity tag. The best crystals obtained belonged to the $P2_1$ space group and diffracted to 2.7 Å. The procedure was repeated with Se-Met-substituted enzyme, and the structure was solved using Se-Met SAD, revealing a *Pt*HmfF hexamer (D_3 symmetry) in the asymmetric unit. Although the UV−vis spectra of the purified enzyme used for crystallization trials indicated the presence of cofactor, no electron density corresponding to the cofactor could be detected in preliminary electron density maps. Final refinement was done using data collected to 2.7 Å on *Pt*HmfF crystals soaked with FMN (as a stable analogue of the prFMN cofactor) in the presence of K^+ and Mn^{2+}, revealing clear electron density for both the FMN and the associated metal ions in the prFMN binding site (Figure S6). The *Pt*HmfF structure is similar to other UbiD family member structures with a Z score of 47 with the bacterial protocatechuate decarboxylase AroY (rmsd 1.6 Å over 441 C-αs),[13] 45 with the *E. coli* UbiD (rmsd 2.5 Å over 440 C-αs),[19] 40 with the fungal cinnamic acid decarboxylase Fdc1 (rmsd 3.1 Å over 440 C-αs)[11] and 38 with recently solved TtnD decarboxylase involved in polyketide biosynthesis (rmsd 2.7 Å over 414 C-αs).[25] The *Pt*HmfF monomer consists of an N-terminal prFMN binding domain connected via an α-helical linker to the oligomerization domain (Figure 5). The C-terminus consists of an extended loop region with some α-helical character that interacts with the prFMN binding domain of an adjacent *Pt*HmfF monomer. An overlay of the six *Pt*HmfF monomers reveals that minor variation occurs in the respective positions of the N-terminal prFMN binding

DOI: 10.1021/acscatal.8b04862
ACS Catal. 2019, 9, 2854−2865

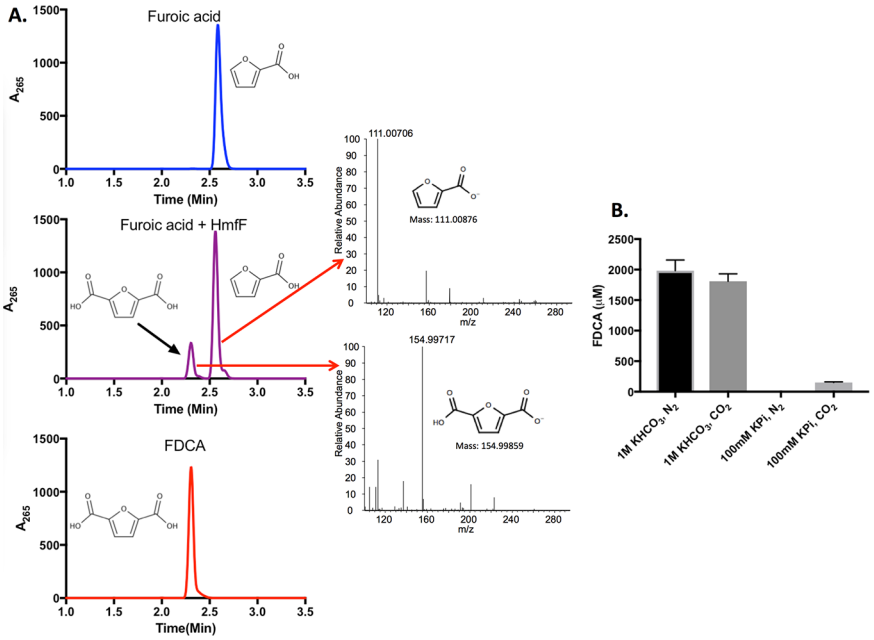

Figure 4. *Pt*HmfF-catalyzed carboxylation of furoic acid to FDCA. (A) HPLC chromatogram demonstrating enzymatic production of FDCA by carboxylation of furoic acid by *P. thermopropionicum* HmfF. Chromatograms of FDCA (red) and 50 mM furoic acid in 1 M $KHCO_3$ solution incubated in the absence (blue) and presence (purple) of the *Pt*HmfF enzyme. Mass spectrometry confirmed that the species that comigrated with the FDCA standard also possessed a mass consistent with FDCA. (B) Furoic acid carboxylation under CO_2 pressure. Assays with or without 1 M $KHCO_3$ were incubated overnight either under N_2 at atmospheric pressure or under CO_2 at 32 bar. Error bars represent SEM, $n = 3$.

domain and the oligomerization domain, suggestive of domain motion via the hinge region connecting both domains (Figure 5B). As the active site (vide infra) is located at the interface between both domains, this could be relevant to catalysis. The phosphate moiety of the bound FMN is coordinated by Mn^{2+} and K^+ ions (the identity of these was derived from the fact they were added to the crystal and was not independently verified), while the isoalloxazine is positioned directly adjacent to the conserved E(D)-R-E ionic network of residues conserved in UbiD (Figure 5C). In the case of *Pt*HmfF, the active site is only partly occluded from solvent as a consequence of the relatively open conformation of the N-terminal prFMN binding domain; this is similar to what has been observed for the canonical UbiD and AroY enzymes (Figure S7). To achieve full occlusion from solvent, as is observed for the fungal Fdc1 enzyme, a hinge motion (akin to that observed by comparison of the various *Pt*HmfF monomers) leading to a closed conformation would be required.

***Pt*HmfF Active Site Contains a Furoic Acid Binding Motif.** All attempts to acquire a crystal structure of the *Pt*HmfF in complex with substrate through either soaking or cocrystallization failed, a possible consequence of the open configuration of the enzyme. Guided by the structure of the related Fdc1 in complex with cinnamic acid substrates,[11] FDCA can easily be placed into the active site of *Pt*HmfF in a similar position with respect to the prFMN cofactor. This positions the substrate furan oxygen approximately within hydrogen-bonding distance of His296 and locates the distal substrate carboxylate adjacent to Arg304 and Arg331. All three putative substrate binding residues are conserved in the HmfF branch of the UbiD family tree (Figure S1). To support our hypothesis regarding the role of H296, R304, and R331 in substrate binding, we made *Pt*HmfF H296N, R304A, and R331A variants. All variants possess UV−vis spectra similar to that of the WT with the exception of the H296N variant (Figure 6A). In the latter case, cofactor related features between 300 and 400 nm are less intense, indicating lower cofactor content. Prolonged incubation of large quantities of protein with substrate resulted in complete decarboxylation of FDCA by WT *Pt*HmfF and the R304A variant (assayed by HPLC). Under these conditions, H296N was able to decarboxylate ∼87% of the substrate, in comparison with 30% using the R331A variant (Figure 6B). Using PDCA as a substrate, only the WT and H296N were able to perform 100% decarboxylation (Figure 6C). A continuous spectrophotometrically based assay (using 1 mM substrate) revealed that all three variants were severely compromised in activity in comparison to the wild type enzyme, with k_{cat} values 30−400 fold lower than the WT against FDCA (Figure 6D). Interestingly, the H296N variant displays a preference for 2,5-pyrroledicarboxylic acid over FDCA and has a slightly higher activity for PDCA in comparison to the WT enzyme (Figure 6D). Michaelis−Menten kinetics revealed that both R304A and H296N variants were not saturated at 1 mM substrate (the maximum possible under the experimental conditions), while no reliable data could be obtained for R331A (Figure 6E). These data clearly indicate the FDCA affinity has been compromised by substitutions at positions H296, R304, and R331.

A Dimeric *Pt*HmfF Variant Binds prFMN but Is Compromised for Activity. The resolution of the hexameric *Pt*HmfF structures obtained is limited and is in sharp contrast to the atomic resolution routinely achieved for the dimeric *A. niger* Fdc1. A structural alignment of *Pt*HmfF hexamer with the related *A. niger* Fdc1 dimer structure demonstrates that *Pt*HmfF A315, N348, F351, T355, A388, F393, V395, and M399 form key hydrophobic interactions between the individual *Pt*HmfF dimers. In Fdc1, the equivalent positions are D343, R382, D385, N389, P424, T429, F431, and R435,

DOI: 10.1021/acscatal.8b04862
ACS Catal. 2019, 9, 2854−2865

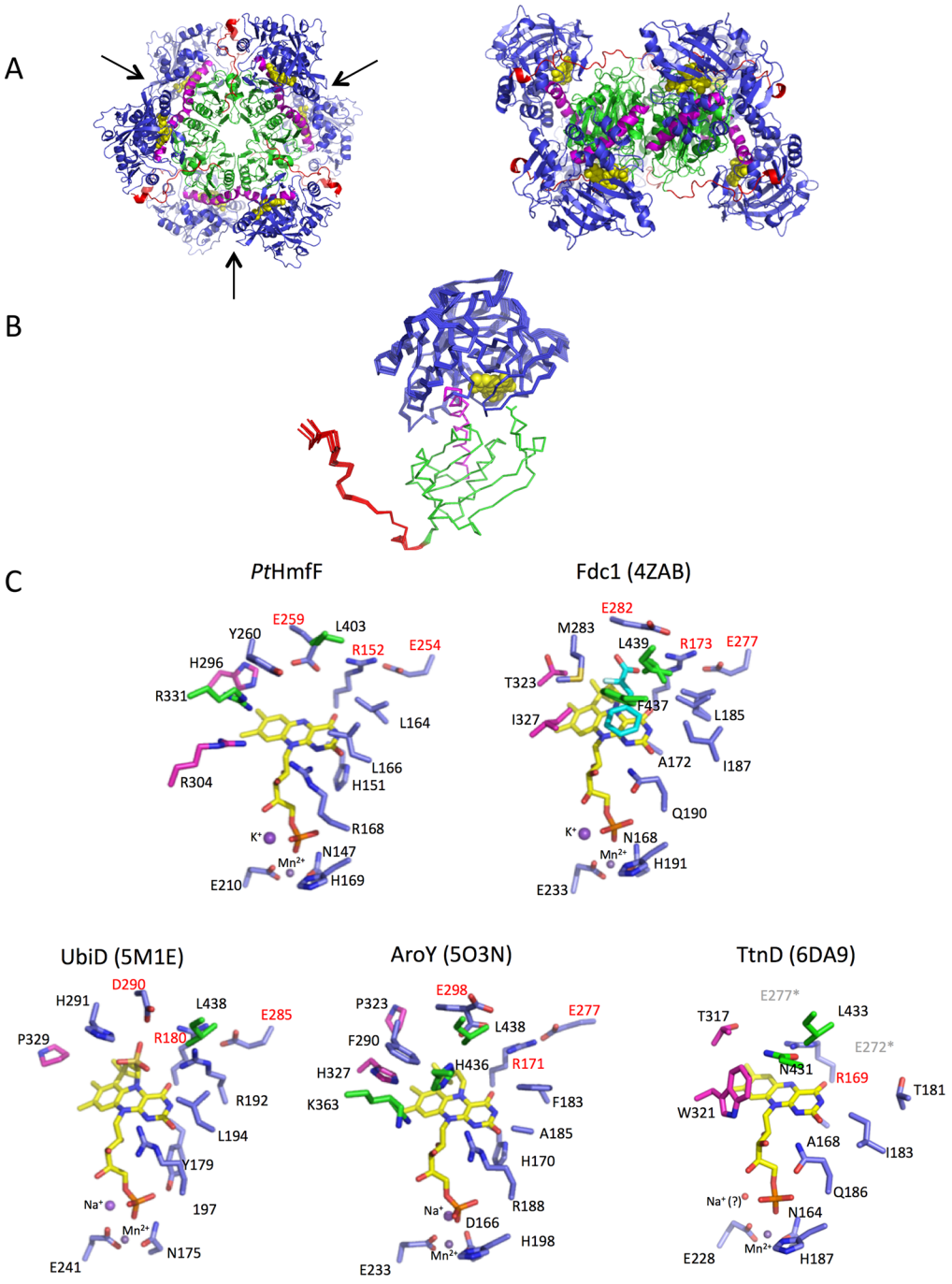

Figure 5. *Pt*HmfF crystal structure. (A) *Pt*HmfF hexamer (D3 symmetry) shown in two orientations, represented in cartoon depiction, with the prFMN binding domain in blue, the connecting helix in magenta, the hexamerization domain in green, and the C-terminal helix in red. The bound FMN is shown as yellow spheres. Arrows indicate the interfaces disrupted by mutagenesis (vide infra). (B) Overlay of the six *Pt*HmfF monomers present in the asymmetric unit with the C-α traces depicted in ribbon using a color coding similar to (A). (C) Side-by-side comparison of the *Pt*HmfF active site with other structurally characterized UbiD family members. Key residues are show in atom color sticks, with carbons colored according to domain structure as used in (A). In the case of the *Aspergillus niger* Fdc1 enzyme, the α-fluorocinnamic acid complex is shown, with the substrate shown in cyan carbons. In the case of the TtnD enzyme, the loop containing residues E272−E277 is not ordered in the FMN-bound structure. The conserved E(D)-R-E motif is highlighted by the use of red labels.

respectively: i.e. generally larger and/or charged residues. We created a *Pt*HmfF variant by substituting for the corresponding *A. niger* Fdc1 amino acids (i.e., A315N, N348R, F351D, T355N, A388P, F393T, V395F, and M399R) to disrupt dimer−dimer interactions. SEC-MALLS of the purified *Pt*HmfF dimer variant indicated a native mass of 110 kDa, broadly consistent with the expected mass of a dimer. Similarly to the WT protein, the purified dimer variant possesses a complex UV−vis spectrum with three main features in the 300−800 nm region (Figure S8). This suggests the presence of prFMN, in addition to minor populations of FMN and the radical prFMN. Despite the presence of prFMN, the dimer variant display weak activity, and incubation of 10 mM FDCA

DOI: 10.1021/acscatal.8b04862
ACS Catal. 2019, 9, 2854−2865

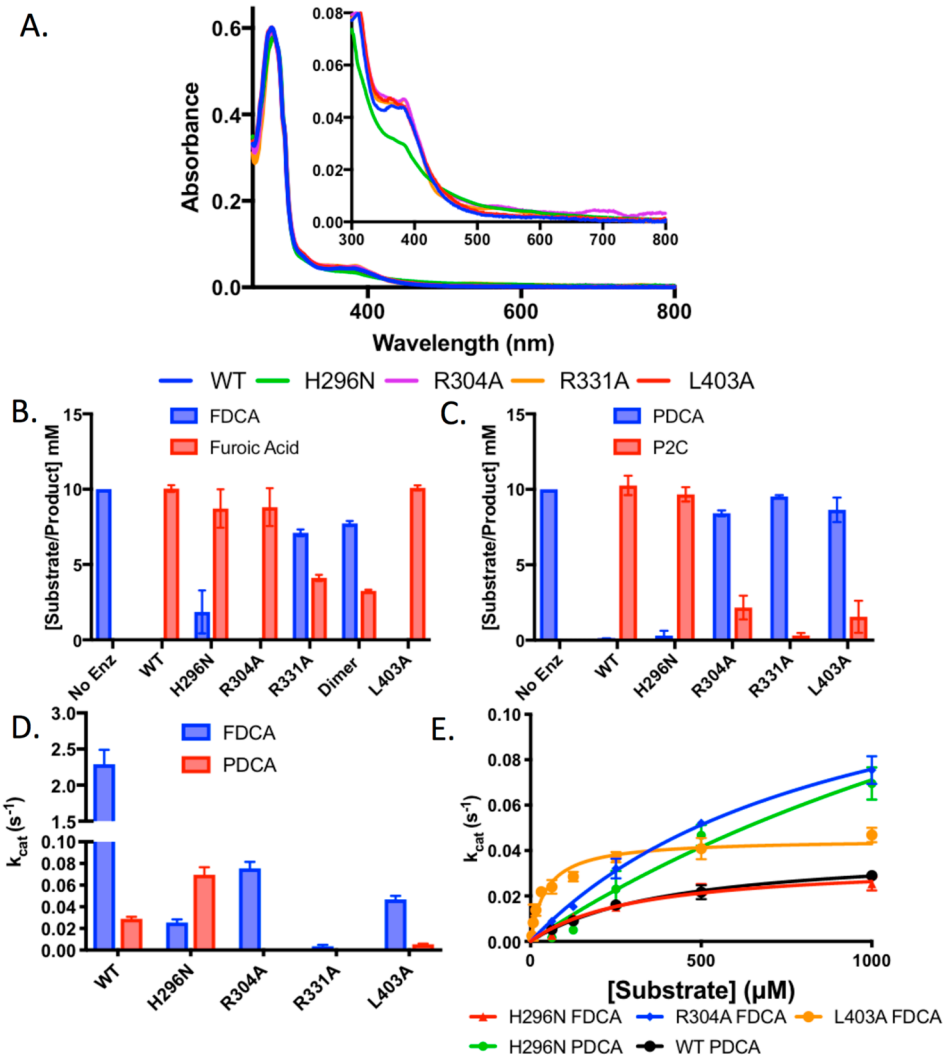

	FDCA		PDCA	
	K_m (μM)	k_{cat} (s^{-1})	K_m (μM)	k_{cat} (s^{-1})
WT	49.4 (±3.7)	2.39 (±0.05)	414 (±63)	0.041 (±0.003)
H296N	312 (±70)	0.035 (±0.003)	2500 (±1500)	0.245 (±0.003)
R304A	918 (±140)	0.15 (±0.02)	-	-
R331A	-	-	-	-
L403A	45.33 (±7.2)	0.045 (±0.002)	ND	ND

Figure 6. Characterization of *Pt*HmfF variants. (A) UV−vis spectra of *Pt*HmfF variants including WT (blue), H296N (green), R304A (magenta), R331A (orange), and L403A (red). Spectra were normalized on the A_{280} peak. The inset shows a closeup of the cofactor-related spectral features present in the 300−800 nm region. (B) Decarboxylation of 10 mM 2,5-furandicarboxylic acid (FDCA) to furoic acid after overnight incubation with *Pt*HmfF variants. (C) Decarboxylation of 10 mM 2,5-pyrroledicarboxylic acid (PDCA) to pyrrole-2-carboxylate after overnight incubation with *Pt*HmfF variants. (D) Rate of decarboxylation of 1 mM FDCA (blue) or 1 mM PDCA (red) by *Pt*HmfF variants. (E) Steady-state kinetics of *Pt*HmfF variants. Error bars represent SEM, $n = 3$.

against 20 μM *Pt*HmfF dimer mutant only resulted in 30% decarboxylation following overnight incubation (Figure 6B).

Crystal Structure of Dimeric *Pt*HmfF Suggests a Key Role for a Conserved Leu in Activity. The *P. thermopropionicum* HmfF dimer variant was crystallized and the structure solved to 2.3 Å using molecular replacement with the WT *Pt*HmfF monomer. Unlike the wild type enzyme, the dimer variant crystals contain prFMN in the active site. Despite the extensive mutation of the WT dimer−dimer interface, the *Pt*HmfF dimer variant is very similar in structure to an individual dimer module from the WT hexamer. The prFMN is bound in a similar position and configuration as the FMN in the *Pt*HmfF hexamer, with little difference in the position of the majority of active site residues. A notable exception is Leu403, which is located on a loop region that is disordered in the *Pt*HmfF dimer variant and therefore absent

DOI: 10.1021/acscatal.8b04862
ACS Catal. 2019, 9, 2854−2865

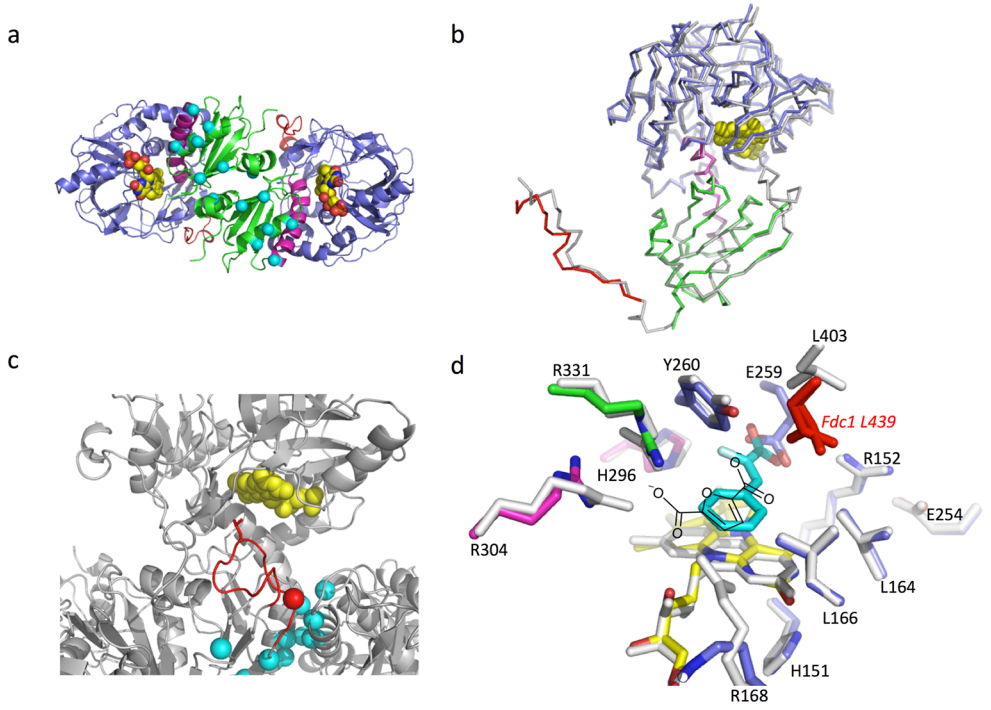

Figure 7. *Pt*HmfF dimer variant crystal structure. (A) *Pt*HmfF dimer variant shown in cartoon representation, with color coding as in Figure 5a. The mutations disrupting the hexamer formation interface are indicated by cyan spheres for the corresponding Cα positions. (B) Overlay of the two *Pt*HmfF monomers present in the asymmetric unit with the Cα traces depicted in ribbon using a color coding similar to that in (A). In addition, a single monomer of the *Pt*HmfF hexamer structure is shown in gray. (C) Position of the Leu403 region (in red) at the prFMN-domain/multimerization domain interface that is disordered in the *Pt*HmfF dimer structure. Mutations at the hexamer formation interface are shown as cyan spheres, except for M399R, which is shown in red. (D) Overlay of the respective *Pt*HmfF hexamer active site (in complex with FMN, in gray) and the *Pt*HmfF dimer variant in complex with prFMN^{iminium}. For comparison, the position of the α-fluorocinnamic acid substrate of *A. niger* Fdc1 with respect the prFMN cofactor is shown (in cyan), as well as the corresponding position of L439 (homologous to *Pt*HmfF L403).

from the active site (Figure 7). The 398−410 region including Leu403 is disordered in both the *Pt*HmfF dimer variant monomers, a likely consequence of the M399R mutation and/or the disruption of the WT dimer−dimer interface. As a consequence, the *Pt*HmfF dimer variant active site is exposed to the solvent. To confirm whether the absence of Leu from the dimer active site contributed to the low activity of the dimer mutant, a L403A *Pt*HmfF was created. While the UV−vis profiles of both WT and the L403A variant are comparable, the latter had a k_{cat} value ~40-fold lower than that of the WT (Figure 6D,E). However, unlike the H296 and R304/331 variants, the L403A K_m value for FDCA was not significantly different from the WT, suggesting that L403 does not contribute to substrate binding. The hydrophobic nature of the carboxylic acid binding pocket has been implicated in the mechanism of other decarboxylases,[26,27] and it is plausible that the highly conserved Leu403 fulfils a similar role. Furthermore, Leu403 is one of the residues most affected by the proposed domain motion (Figure 5B and Figure S7) that occludes the *Pt*HmfF active site from solvent.

Proposed Mechanism for HmfF. Previous studies for the Fdc1 enzyme have suggested that the reversible decarboxylation occurs via a 1,3-dipolar cycloaddition between substrate and prFMN. In principle, a similar reaction scheme can be proposed for any of the UbiD substrates. However, for those substrates where (de)carboxylation occurs directly on an aromatic ring system, cycloaddition also requires dearomatization. An alternative proposal has been put forward for AroY, on the basis of formation of a quinoid intermediate that allows formation of a substrate−prFMN adduct. In view of the modest aromatic nature of the furan ring, an FDCA or furoic acid adduct with prFMN could be formed through either cycloaddition (Ib in Figure 8) or via formation of an oxonium ion (Ia in Figure 8) in the case of HmfF. Chemical precedent exists for the 1,3-cycloaddition of furans to 1,3-dipoles.[28] It is unclear at present which route is preferred for HmfF, and this will require further investigation. However, it is interesting to note that HmfF-catalyzed H/D exchange can be readily observed for weakly aromatic heteroaromatic acids only at those positions that are adjacent to a carbon, hinting at the possibility that species Ib is indeed formed during the enzyme reaction. Furthermore, neither decarboxylation of the more aromatic thiophenedicarboxylic acid nor H/D exchange of thiophene-2-carboxylate was observed. In fact, thiophene compounds are not known to readily undergo cycloaddition reactions, in contrast to furan. While HmfF is able to catalyze furoic acid carboxylation under ambient conditions, this requires a mechanism for increasing [CO_2]. Other decarboxylases have been found to catalyze pyrrole carboxylation in supercritical CO_2,[29] and we intend to explore whether HmfF (natural or evolved variants) can be used under these conditions. Further studies will also need to address cofactor stability and homogeneity to ensure a robust biocatalyst for the carboxylation of furoic acid.

METHODS

Cloning of *Pelotomaculum thermopropionicum* and *Geobacillus kaustophilus* HmfF for *E. coli* Heterologous Expression. The *P. thermopropionicum* 2,5-furandicarboxylic acid decarboxylase (HmfF) gene (WP_012031668), and *G.*

DOI: 10.1021/acscatal.8b04862
ACS Catal. 2019, 9, 2854−2865

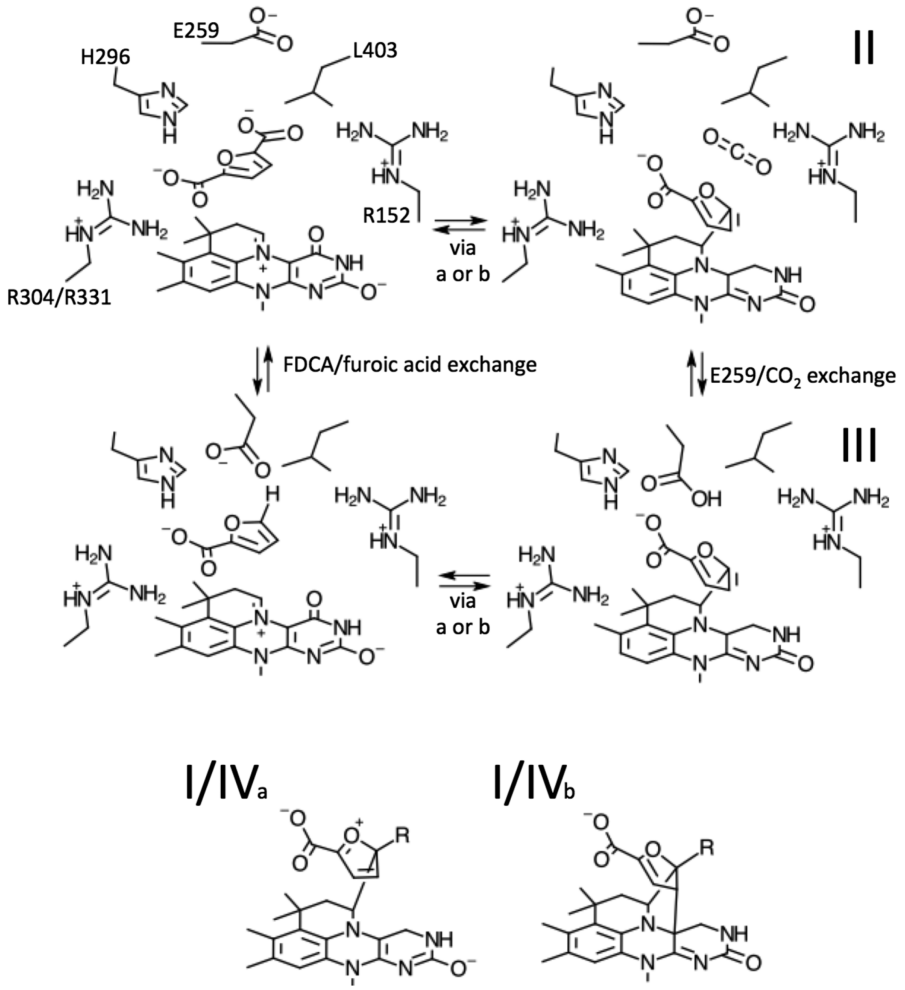

Figure 8. Proposal for the HmfF mechanism. The HmfF substrate is bound by polar interactions with the HmfF specific R304/R331 and H296, in addition to the UbiD family conserved R152 (part of the UbiD Glu-Arg-Glu motif). Substrate binding is possibly linked to domain motion, affecting the relative position of L403 and R331. Formation of a covalent prFMN^{iminium}–substrate adduct can occur either through nucleophilic attack, leading to species Ia, or through cycloaddition, leading to species Ib. Decarboxylation of either species leads to intermediate II, following E260/CO_2 exchange; protonation of the substrate via E260 leading to product release occurs through either intermediate IVa or IVb.

kaustophilus HmfF gene (WP_011229502) were codon optimized for *E. coli* and synthesized (Genscript). The *G. kaustophilus* HmfF gene was synthesized with *Nde*I and *Xho*I restriction sites upstream and downstream of the coding region, respectively. The gene was excised from the pUC57 plasmid using *Nde*I and *Xho*I (NEB) and purified using a QIAquick gel extraction kit (Qiagen). The insert was ligated in to *Nde*I/*Xho*I linearized pET30a (MerckMillipore) using T4 ligase (NEB).

The *P. thermopropionicum* HmfF gene was amplified using Phusion polymerase (NEB) and the primers Ptherm30aF (AAGGAGATATACATATGTCCCACTCCCTGCG) and Ptherm30aR (GGTGGTGGTGCTCGAGTTCCAGGTAG-TCTGCCAG) (Eurofins), and the PCR product was cloned into pET30a (MerckMillipore) linearized with *Nde*I and *Xho*I (NEB) using Infusion HD (Clontech) and transformed into *E. coli* NEB5α(NEB). The plasmid was transformed into *E. coli* BL21(DE3) (NEB) either on its own or cotransformed with ubiXpET21b as described previously.[11]

Mutagenesis. Mutagenesis primers were designed using the QuikChange Primer Design Program (http://www.genomics.agilent.com/primerDesignProgram.jsp). PCR was performed using Phusion polymerase (NEB). Template DNA was removed by *Dpn*I (NEB) digest, and the PCR product was transformed into *E. coli* NEB5α. Once the presence of the desired mutation was confirmed by DNA sequencing, the plasmid was cotransformed with ubiXpET21b into *E. coli* BL21(DE3).

Expression and Purification of His-Tagged HmfF Proteins. The various HmfF enzymes were expressed in BL21(DE3) grown at 37 °C/180 rpm in LB broth supplemented with 50 μg/mL kanamycin and 50 μg/mL ampicillin. At mid log phase cells were induced with 0.25 mM IPTG and supplemented with 1 mM $MnCl_2$, grown overnight at 15 °C/180 rpm and then harvested by centrifugation (4 °C, 7000*g* for 10 min). Cell pellets were resuspended in buffer A (200 mM KCl, 1 mM $MnCl_2$, 50 mM Tris pH 7.5) supplemented with DNase, RNase, lysozyme (Sigma), and Complete EDTA-free protease inhibitor cocktail (Roche). Cells were lysed using a French press at 20000 psi, and the lysate was clarified by centrifugation at 125000*g* for 90 min. The supernatant was applied to a Ni-NTA agarose column (Qiagen). The column washed with three column volumes of buffer A supplemented with 10 mM imidazole, and the protein eluted in 1 mL fractions with buffer A supplemented with 250 mM imidazole. Samples were subjected to SDS-PAGE analysis,

DOI: 10.1021/acscatal.8b04862
ACS Catal. 2019, 9, 2854–2865

and fractions found to contain the purified protein were pooled. Imidazole was removed using a 10-DG desalting column (Bio-Rad) equilibrated with buffer A. Protein was aliquoted and flash frozen until required. Where necessary, HmfF Ni^{2+}-affinity purification was performed anaerobically within a ~100% N_2 atmosphere glovebox (Belle Technology, U.K.).

Production and Purification of Untagged *P. thermopropionicum* HmfF. For the purposes of crystallization and structural characterization untagged PtHmfF was used. To produce untagged *P. thermopropionicum*, HmfF the gene was amplified using the primers Ptherm21bF (AAGGAGATATACATATGTCCCACTCCCTGCG) and Ptherm21bR (GGTGGTGGTGCTCGAGTTATTATTCCAGGTAGTCTGCCAG) and cloned into *Nde*I/*Xho*I linearized with pET21b (MerckMillipore). The UbiX gene was amplified using the primers UbiXF (AGGAGATATACCATGGGGTCAGGTCC) and UbiXR (CTTTACCAGACTCGAGTTATTCGTCTGAAACCAGGTGTTG) and cloned into pCDF (MerckMillipore) linearized with *Nco*I and *Xho*I.

Once the sequence of the desired insert was confirmed, the corresponding purified plasmids were cotransformed into *E. coli* BL21(DE3).

Protein expression was performed as described above, except the antibiotics used were 50 μg/mL streptomycin and 50 μg/mL ampicillin. Cell pellets were resuspended in buffer A (200 mM KCl, 1 mM $MnCl_2$, 50 mM Tris pH 7.5) supplemented with DNase, RNase, lysozyme (Sigma), and Complete EDTA-free protease inhibitor cocktail (Roche). Cells were lysed using a French press at 20000 psi, and the lysate was incubated at 50 °C for 30 min to precipitate host proteins. The lysate was clarified by centrifugation at 125000*g* for 90 min. The *P. thermopropionicum* HmfF was precipitated with 30% saturated ammonium sulfate at 4 °C, the supernatant was removed following centrifugation, the pellet was solubilized in buffer A and subjected to size exclusion chromatography using a HiPrep S200 column (GE Healthcare) equilibrated with buffer A, and 2 mL fractions were collected. Samples were subjected to SDS-PAGE analysis, and fractions found to contain the purified protein were pooled. Protein was aliquoted and flash-frozen until required.

Expression of Selenomethionine-Labeled HmfF. Untagged *P. thermopropionicum* HmfF was expressed in non-auxotrophic Bl21(DE3) and labeled with selenomethionine by growth on amino acids known to inhibit the methionine biosynthesis pathway.[30] Precultures grown in LB media were inoculated into M9 media supplemented with 0.4% glucose, 50 μg/mL streptomycin, and 50 μg/mL ampicillin. At mid log phase cultures were further supplemented with phenylalanine, lysine, and threonine (100 mg/L), isoleucine, leucine, valine (50 mg/L), and 60 mg/L selenomethionine. Cells were induced with 0.25 mM IPTG and grown overnight at 15 °C/180 rpm and then harvested by centrifugation (4 °C, 7000*g* for 10 min).

***P. thermopropionicum* HmfF Dimer Mutant Cloning, Protein Expression, and Purification.** The *Pelotomaculum thermopropionicum* HmfF gene with eight substitutions designed to disrupt the trimer of dimers (A315N, N348R, F351D, T355N, A388P, F393T, V395F, M399R) was codon-optimized to remove codons that were rare in *E. coli* and synthesized (GeneArt). The gene was amplified by PCR using the primers PtDimer_28aF (CGCGCGGCAGCCATATGAGCCATAGCCTGCG) and PtDimer_28aR (GGTGGTGGTGCTCGAGTTATTATTCCAGATAATCGGCCAG) and cloned in to pET28a linearized with *Nde*I and *Xho*I using Infusion (Clontech). Protein was expressed and purified by Ni affinity as described above before being subjected to size exclusion chromatography using a HiPrep S200 column (GE Healthcare) equilibrated with buffer A, and 2 mL fractions were collected.

UV−Vis Spectroscopy and Protein Quantification. UV−vis absorbance spectra were recorded with a Cary UV−vis spectrophotometer. The protein concentration was estimated from the A_{280} absorption peak with extinction coefficients calculated from the primary amino acid sequence using the ProtParam program on the ExPASy proteomics server. *P. thermopropionicum* HmfF was estimated using ε_{280} = 28420 M^{-1} cm^{-1} and *G. kaustophilus* HmfF using ε_{280} = 31860 M^{-1} cm^{-1}.

HmfF Decarboxylation Assays Monitored by UV−Vis. Initial rates of FDCA decarboxylation were determined by UV−vis spectroscopy at 265 nm using the extinction coefficient ε_{265} = 18000 M^{-1} cm^{-1}, using a Cary 50 Bio spectrophotometer (Varian). Assays were performed against various concentrations of substrate in 350 μL of 50 mM KCl, 50 mM NaPi pH 6 in a 1 mm path length cuvette at 50 °C.

HmfF Decarboxylation Assays Monitored by HPLC. Typical assays containing 500 μL of 10 mM substrate in 50 mM KCl, 50 mM NaPi pH 6 with or without enzyme (typically 20 μM) were set up in an anaerobic glovebox in 2 mL crimp-seal vials before being removed to a 50 °C incubator. After incubation, 50 μL of the sample was added to 450 μL of 50% v/v H_2O/acetonitrile and centrifuged at 16100*g* to remove precipitate. Sample analysis was performed using an Agilent 1260 Infinity Series HPLC equipped with a UV detector. The stationary phase was a Kinetex 5 μm C18 100A column, 250 × 4.6 mm. The mobile phase was acetonitrile/water (50/50) with 0.1% trifluoroacetic acid (TFA) at a flow rate of 1 mL/min, and unless otherwise stated, detection was performed at a wavelength of 265 nm.

HmfF Carboxylation Reactions Assayed by HPLC/HPLC-MS. Assays containing 50 mM furoic acid, 100 mM KPi pH6, 1 M $KHCO_3$ (final pH 7.5) were incubated with and without HmfF enzyme at 50 °C overnight. The sample was centrifuged at 16100*g* to remove precipitate and 10 μL added to 490 μL of 50% v/v H_2O/acetonitrile. Sample analysis was typically performed by HPLC as described above. For carboxylation under pressurized CO_2, reaction mixtures were set up as above and then placed in an Asynt 250 mL stainless-steel autoclave pressurized to 32 bar with CO_2 which was incubated at 50 °C overnight. Before the pressure was released, the temperature was increased to 100 °C for 10 min to denature the enzyme.

LC-MS was performed to confirm the identity of the carboxylation product. The reaction was carried out as above but with ammonium bicarbonate in place of $KHCO_3$. Analysis was performed using UHPLC (Dionex ultimate 3000) combined with high-resolution mass spectrometry (Thermo Scientific Q Exactive Plus). The samples were run under the negative mode. For the full scan, the mass spectrometry scan range was set as m/z 50−300: resolving power 50000 (fwhm at m/z 200), spray voltage 3 kV, capillary temperature 250 °C, capillary voltage 25 V, tube lens voltage 170 V, skimmer voltage 36 V. Mobile phase A (0.05% formic acid, H_2O) and mobile phase B (0.05% formic acid, acetonitrile) were used for separating the samples; the mobile phase started from 5% B

DOI: 10.1021/acscatal.8b04862
ACS Catal. 2019, 9, 2854−2865

and increased to 95% B in 3 min, and the flow rate was 0.6 mL/min.

^{1}H NMR Monitored Enzyme Catalyzed Deuterium Exchange. A mixture of 10 mM substrate and 100 mM NaPi pD 6.4 in D_2O was incubated overnight at 50 °C with and without 10 μM HmfF. Data were collected at 298 K on a Bruker 500 MHz NMR AVIII spectrometer with QCI-F cryprobe, using the noesygppr1d pulse sequence with 3 s acquisition time plus 1 s recycle delay, accumulating 32 scans.

Size Exclusion Chromatography Coupled to Multi-Angle Light Scattering (SEC-MALS). Size exclusion chromatography coupled with multiangle light scattering (SEC-MALS) analysis was performed at 25 °C. A 500 μL portion of 1.5 mg/mL protein was loaded onto a size exclusion column (for the native protein a Superose 6 10/300 GL column was used and for the dimer mutant a Superdex 200 10/300GL column (GE Life Sciences)), equilibrated in 200 mM KCl, 1 mM $MnCl_2$, 50 mM Tris pH 7.5 and a flow rate of 0.75 mL/min. Eluting samples were passed through a Wyatt DAWN Heleos II EOS 18-angle laser photometer coupled to a Wyatt Optilab rEX refractive index detector. Data were analyzed using Astra 6 software (Wyatt Technology Corp., CA, USA).

Enzyme Reconstitution in Vitro. Reconstitution was performed anaerobically within a 100% N_2 atmosphere glovebox (Belle Technology, UK). *Holo*-PtHmfF was obtained by reconstituting singly expressed HmfF with reduced prFMN under anaerobic conditions as described previously.[19] Reaction of a mixture consisting of 1 mM FMN, 2 mM DMAP (Sigma), 50 μM Fre reductase, and 50 μM UbiX in buffer A was started by the addition of 5 mM NADH. Following incubation, the reaction mixture was filtered through a 10k MWCO centrifugal concentrator to remove UbiX and Fre proteins. The filtrate containing the prFMN product was used to reconstitute anaerobic *apo*-HmfF in a 2:1 molar ratio, with excess cofactor being removed using a PD25 desalting column (GE Healthcare) equilibrated with buffer A. Enzyme assays were performed by UV−vis spectroscopy using a Cary 50 Bio spectrophotometer (Varian) as described above.

CD Monitored Thermal Changes in PtHmfF. A 2 mg/mL PtHmfF sample in 50 mM KCl, 50 mM NaPi pH6 was used. Circular dichroism spectra were recorded between 190 and 260 nm in a 0.1 mm path length cuvette using an Applied Photophysics Chirascan CD spectrophotometer. The temperature was ramped from 20 to 95 °C in 5 °C increments with 2 min equilibration time before each measurement.

Crystallization of PtHmfF and PtHmfF Dimer Variant. Purified *Pelotomaculum thermopropionicum* HmfF in 100 mM NaCl, 25 mM Tris, pH 7.5 was concentrated in a Vivaspin 30 kDa cut off spin concentrator to a final concentration of 11 mg/mL. Initial screening by sitting drop vapor diffusion was performed; mixing 0.3 μL of protein with 0.3 μL of mother liquor led to crystals under a variety of conditions on incubation at 21 °C. The best-performing crystals originated from column 10 of the Morpheus commercial screen (Molecular Dimensions) consisting of 0.1 M Tris/BICINE buffer pH 8.5, 20% v/v ethylene glycol, and 10% w/v PEG 8000. Crystals of the *P. thermopropionicum* HmfF dimer mutant were attained as above but were grown at 4 °C in condition D6 of the Morpheus screen (Molecular Dimensions) consisting of 0.12 M alcohols, 0.1 M NaHEPES/MOPS buffer pH 7.5, 20% v/v ethylene glycol, and 10% w/v PEG 8000.

Diffraction Data Collection and Structure Elucidation. Crystals were flash-cooled in liquid nitrogen. Data were collected at the Diamond beamlines and subsequently handled using the CCP4 suite.[22] All data were reduced and scaled using XDS.[31] Interpretable maps were obtained from Se-Met-substituted crystals following 6-fold NCS averaging using DM.[32] An initial model was automatically generated using Buccaneer[32] and iteratively rebuilt and refined using Coot and REFMAC5.[32] The final model was refined using data extending to 2.7 Å for a crystal soaked with FMN with six monomers in the asymmetric unit. The structure of the prFMN containing HmfF dimer mutant was solved using molecular replacement with the HmfF wild type structure as a search model and iteratively rebuilt and refined using Coot and REFMAC5. For final data and refinement statistics see Table S1.

■ ASSOCIATED CONTENT

Supporting Information

The Supporting Information is available free of charge on the ACS Publications website at DOI: 10.1021/acscatal.8b04862.

Crystallographic table of data collection and refinement statistics, phylogenetic tree of UbiD/Fdc1 family decarboxylases, production of soluble and active HmfF, PtHmfF enzyme stability, circular dichroism spectra of *Pt*HmfF, HmfF H/D exchange monitored by NMR, electron density for bound cofactor and metal ions in PtHmF, overlay of crystal structures of UbiD enzyme family members, and UV−vis spectra obtained for the *P. thermopropionicum* HmfF dimer mutant (PDF)

■ AUTHOR INFORMATION

Corresponding Author

*D.L.: tel, 0044 161 306 51 50; e-mail, david.leys@manchester.ac.uk.

ORCID

Karl A.P. Payne: 0000-0002-6331-6374
Cunyu Yan: 0000-0002-3603-2421
Igor Larrosa: 0000-0002-5391-7424
David Leys: 0000-0003-4845-8443

Author Contributions

D.L. conceived and coordinated the study. K.A.P.P. carried out experiments with help from K.F. and S.A.M. S.A.M. performed in vitro reconstitution of HmfF with UbiX. M.J.C. performed NMR. C.Y. performed LC-MS. D.J.H. assisted with CD data collection and analysis. D.M.C. and I.L. advised and performed carboxylation reactions under pressurized CO_2. D.L. wrote the paper. All authors reviewed the results and approved the final version of the manuscript.

Notes

The authors declare no competing financial interest.

■ ACKNOWLEDGMENTS

This work was supported by the BBSRC grant BB/K017802 and ERC pre-FAB 695013. The atomic coordinates and structure factors (codes 6H6V and 6H6X) have been deposited to the Protein Data Bank (http://www.pdb.org). The authors acknowledge the assistance given by the use of the Manchester Protein Structure Facility and by T. Jowitt and H. Ruiz-Nivia of the Biomolecular Analysis Facility for performing SEC-MALS. We thank Diamond Light Source for access

DOI: 10.1021/acscatal.8b04862
ACS Catal. 2019, 9, 2854−2865

(proposal numbers MX12788 and MX17773) that contributed to the results presented here. D.L. is a Royal Society Wolfson Merit Award holder.

REFERENCES

(1) Werpy, T., Petersen, G. Top value added chemicals from biomass. In *Results of Screening for Potential Candidates from Sugars and Synthesis Gas*; Vol. *1*, pp 26−28; http://www.nrel.gov/docs/fy04osti/35523.pdf, accessed October 2018 (US DOE, 2004).

(2) Eerhart, A. J. J. E.; Faaij, A. P. C.; Patel, M. K. Replacing Fossil Based PET with Biobased PEF; Process Analysis, Energy and GHG Balance. *Energ. Energy Environ. Sci.* **2012**, *5*, 6407−6422.

(3) Banerjee, A.; Dick, G. R.; Yoshino, T.; Kanan, M. W. Carbon Dioxide Utilization via Carbonate-promoted C-H Carboxylation. *Nature* **2016**, *531*, 215−221.

(4) Moreau, C.; Belgacem, M. N.; Gandini, A. Recent Catalytic Advances in the Chemistry of Substituted Furans from Carbohydrates and in the Ensuing Polymers. *Top. Catal.* **2004**, *27*, 11−30.

(5) Lange, J. P.; van der Heide, E.; van Buijtenen, J.; Price, R. Furfural—a Promising Platform for Lignocellulosic Biofuels. *ChemSusChem* **2012**, *5*, 150−166.

(6) Wierckx, N.; Koopman, F.; Bandounas, L.; de Winde, J. H.; Ruijssenaars, H. J. Isolation and characterization of *Cupriavidus basilensis* HMF14 for biological removal of inhibitors from lignocellulosic hydrolysate. *Microb. Biotechnol.* **2010**, *3*, 336−343.

(7) Koopman, F.; Wierckx, N.; de Winde, J. H.; Ruijssenaars, H. J. Identification and Characterization of the Furfural and 5-(Hydroxymethyl)furfural Degradation Pathways of *Cupriavidus basilensis* HMF14. *Proc. Natl. Acad. Sci. U. S. A.* **2010**, *107*, 4919−4924.

(8) Marshall, S. A.; Payne, K. A. P.; Leys, D. The UbiX-UbiD system: The Biosynthesis and Use of Prenylated Flavin (prFMN). *Arch. Biochem. Biophys.* **2017**, *632*, 209−221.

(9) Leys, D. Flavin Metamorphosis: Cofactor Transformation through Prenylation. *Curr. Opin. Chem. Biol.* **2018**, *47*, 117−125.

(10) White, M. D.; Payne, K. A.; Fisher, K.; Marshall, S. A.; Parker, D.; Rattray, N. J.; Trivedi, D. K.; Goodacre, R.; Rigby, S. E.; Scrutton, N. S.; Hay, S.; Leys, D. UbiX is a Flavin Prenyltransferase Required for Bacterial Ubiquinone Biosynthesis. *Nature* **2015**, *522*, 502−506.

(11) Payne, K. A.; White, M. D.; Fisher, K.; Khara, B.; Bailey, S. S.; Parker, D.; Rattray, N. J.; Trivedi, D. K.; Goodacre, R.; Beveridge, R.; Barran, P.; Rigby, S. E.; Scrutton, N. S.; Hay, S.; Leys, D. New Cofactor Supports alpha, beta-unsaturated Acid Decarboxylation via 1,3-Dipolar Cycloaddition. *Nature* **2015**, *522*, 497−501.

(12) Meckenstock, R. U.; Boll, M.; Mouttaki, H.; Koelschbach, J. S.; Cunha Tarouco, P.; Weyrauch, P.; Dong, X.; Himmelberg, A. M. Anaerobic Degradation of Benzene and Polycyclic Aromatic Hydrocarbons. *J. Mol. Microbiol. Biotechnol.* **2016**, *26*, 92−11.

(13) Payer, S. E.; Marshall, S. A.; Barland, N.; Sheng, X.; Reiter, T.; Dordic, A.; Steinkellner, G.; Wuensch, C.; Kaltwasser, S.; Fisher, K.; Rigby, S. E. J.; Macheroux, P.; Vonck, J.; Gruber, K.; Faber, K.; Himo, F.; Leys, D.; Pavkov-Keller, T.; Glueck, S. M. Regioselective para-Carboxylation of Catechols with a Prenylated Flavin Dependent Decarboxylase. *Angew. Chem., Int. Ed.* **2017**, *56*, 13893−13897.

(14) Lupa, B.; Lyon, D.; Gibbs, M. D.; Reeves, R. A.; Wiegel, J. Distribution of Genes Encoding the Microbial Non-Oxidative Reversible Hydroxyarylic Acid Decarboxylases/Phenol Carboxylases. *Genomics* **2005**, *86*, 342−351. 2005

(15) Koopman, F.; Wierckx, N.; de Winde, J. H.; Ruijssenaars, H. J. Efficient Whole-Cell Biotransformation of 5-(Hydroxymethyl)furfural into FDCA, 2,5-Furandicarboxylic Acid. *Bioresour. Technol.* **2010**, *101*, 6291−6296.

(16) Hayakawa, H.; Motoyama, K.; Sobue, F.; Ito, T.; Kawaide, H.; Yoshimura, T.; Hemmi, H. Modified Mevalonate Pathway of the Archaeon *Aeropyrum pernix* Proceeds via *trans*-anhydromevalonate 5-phosphate. *Proc. Natl. Acad. Sci. U. S. A.* **2018**, *115*, 10034−10039.

(17) Wierckx, N.; Koopman, F.; Ruijssenaars, H. J.; de Winde, J. H. Microbial Degradation of Furanic Compounds: Biochemistry, Genetics, and Impact. *Appl. Microbiol. Biotechnol.* **2011**, *92*, 1095−1105.

(18) Takami, H.; Takaki, Y.; Chee, G. J.; Nishi, S.; Shimamura, S.; Suzuki, H.; Matsui, S.; Uchiyama, I. Thermoadaptation Trait Revealed by the Genome Sequence of Thermophilic *Geobacillus kaustophilus*. *Nucleic Acids Res.* **2004**, *32*, 6292−6303.

(19) Marshall, S. A.; Fisher, K.; Ni Cheallaigh, A.; White, M. D.; Payne, K. A.; Parker, D. A.; Rigby, S. E.; Leys, D. Oxidative Maturation and Structural Characterization of Prenylated FMN Binding by UbiD, a Decarboxylase Involved in Bacterial Ubiquinone Biosynthesis. *J. Biol. Chem.* **2017**, *292*, 4623−4637.

(20) Bailey, S. S.; Payne, K. A. P.; Fisher, K.; Marshall, S. A.; Cliff, M. J.; Spiess, R.; Parker, D. A.; Rigby, S. E. J.; Leys, D. The Role of Conserved Residues in Fdc Decarboxylase in Prenylated Flavin Mononucleotide Oxidative Maturation, Cofactor Isomerization, and Catalysis. *J. Biol. Chem.* **2018**, *293*, 2272−2287.

(21) Ferguson, K. L.; Arunrattanamook, N.; Marsh, E. N. Mechanism of the Novel Prenylated Flavin-Containing Enzyme Ferulic Acid Decarboxylase Probed by Isotope Effects and Linear Free-Energy Relationships. *Biochemistry* **2016**, *55*, 2857−2863.

(22) Luo, F.; Gitiafroz, R.; Devine, C. E.; Gong, Y.; Hug, L. A.; Raskin, L.; Edwards, E. A. Metatranscriptome of an Anaerobic Benzene-Degrading, Nitrate-reducing Enrichment Culture Reveals involvement of Carboxylation in Benzene Ring Activation. *Appl. Environ. Microbiol.* **2014**, *80*, 4095−4107.

(23) Abu Laban, N.; Selesi, D.; Rattei, T.; Tischler, P.; Meckenstock, R. U. Identification of Enzymes Involved in Anaerobic Benzene Degradation by a Strictly Anaerobic Iron-Reducing Enrichment Culture. *Environ. Microbiol.* **2010**, *12*, 2783−2796.

(24) Schuhle, K.; Fuchs, G. Phenylphosphate carboxylase: a New C-C Lyase Involved in Anaerobic Phenol Metabolism in *Thauera aromatica*. *J. Bacteriol.* **2004**, *186*, 4556−4567.

(25) Annaval, T.; Han, L.; Rudolf, J. D.; Xie, G.; Yang, D.; Chang, C. Y.; Ma, M.; Crnovcic, I.; Miller, M. D.; Soman, J.; Xu, W.; Phillips, G. N.; Shen, B. Biochemical and Structural Characterization of TtnD, a Prenylated FMN-dependent Decarboxylase from the Tautomycetin Biosynthetic Pathway. *ACS Chem. Biol.* **2018**, *13*, 2728−2738.

(26) Okrasa, K.; Levy, C.; Wilding, M.; Goodall, M.; Baudendistel, N.; Hauer, B.; Leys, D.; Micklefield, J. Structure and Mechanism of an Unusual Malonate Decarboxylase and Related Racemases. *Chem. - Eur. J.* **2008**, *14*, 6609−6613.

(27) Jez, J. M.; Ferrer, J. L.; Bowman, M. E.; Dixon, R. A.; Noel, J. P. Dissection of Malonyl-coenzyme A Decarboxylation from Polyketide Formation in the Reaction Mechanism of a Plant Polyketide Synthase. *Biochemistry* **2000**, *39*, 890−902.

(28) Tsuge, O.; Ueno, K.; Kanemasa, S. Intramolecular 1,3-dipolar Cycloadditions to a Furan Ring. *Chem. Lett.* **1984**, *13*, 285−288.

(29) Wieser, M.; Fuji, N.; Yoshida, T.; Nagasawa, T. Carbon Dioxide Fixation by Reversible Pyrrole-2-carboxylate Decarboxylase from *Bacillus megaterium* PYR2910. *Eur. J. Biochem.* **1998**, *257*, 495−499.

(30) Van Duyne, G. D.; Standaert, R. F.; Karplus, P. A.; Schreiber, S. L.; Clardy, J. Atomic Structures of the Human Immunophilin FKBP-12 Complexes with FK506 and Rapamycin. *J. Mol. Biol.* **1993**, *229*, 105−124.

(31) Kabsch, W. Xds. *Acta Crystallogr., Sect. D: Biol. Crystallogr.* **2010**, *66*, 125−132.

(32) Winn, M. D.; Ballard, C. C.; Cowtan, K. D.; Dodson, E. J.; Emsley, P.; Evans, P. R.; Keegan, R. M.; Krissinel, E. B.; Leslie, A. G.; McCoy, A.; McNicholas, S. J.; Murshudov, G. N.; Pannu, N. S.; Potterton, E. A.; Powell, H. R.; Read, R. J.; Vagin, A.; Wilson, K. S. Overview of the CCP4 Suite and Current Developments. *Acta Crystallogr., Sect. D: Biol. Crystallogr.* **2011**, *67*, 235−242.

DOI: 10.1021/acscatal.8b04862
ACS Catal. 2019, 9, 2854−2865